

# Effects of dilution in a 2D topological magnon insulator

Miguel S. Oliveira,<sup>1</sup> T. V. C. Antão,<sup>2</sup> Eduardo V. Castro,<sup>1,3</sup> and Nuno Peres<sup>4,5,6</sup>

<sup>1</sup>*Centro de Física das Universidades do Minho e do Porto, LaPMET,  
Departamento de Física e Astronomia, Faculdade de Ciências,  
Universidade do Porto, 4169-007 Porto, Portugal*

<sup>2</sup>*Laboratório de Instrumentação e Física Experimental de Partículas (LIP), University of Minho, 4710-057 Braga, Portugal*

<sup>3</sup>*Beijing Computational Science Research Center, Beijing 100084, China*

<sup>4</sup>*Centro de Física das Universidades do Minho e do Porto (CF-UM-UP) e Departamento de Física,  
Universidade do Minho, P-4710-057 Braga, Portugal*

<sup>5</sup>*International Iberian Nanotechnology Laboratory (INL),  
Av Mestre José Veiga, 4715-330 Braga, Portugal*

<sup>6</sup>*POLIMA—Center for Polariton-driven Light-Matter Interactions,  
University of Southern Denmark, Campusvej 55, DK-5230 Odense M, Denmark*

We study the effect of diluting a two-dimensional ferromagnetic insulator hosting a topological phase in the clean limit. By considering the ferromagnetic Heisenberg model in the honeycomb lattice with second nearest-neighbor Dzyanishkii-Moriya interaction, and working in the linear spin-wave approximation, we establish the topological phase diagram as a function of the fraction  $p$  of diluted magnetic atoms. The topological phase with Chern number  $C = 1$  is robust up to a moderate dilution  $p_1^*$ , while above a higher dilution  $p_2^* > p_1^*$  the system becomes trivial. Interestingly, both  $p_1^*$  and  $p_2^*$  are below the classical percolation threshold  $p_c$  for the honeycomb lattice, which gives physical significance to the obtained phases. In the topological phase for  $p < p_1^*$ , the magnon spectrum is gapless but the states filling the topological, clean-limit gap region are spatially localized. For energies above and below the region of localized states, there are windows composed of extended states. This is at odds with standard Chern insulators, where extended states occur only at single energies. For dilutions  $p_1^* < p < p_2^*$ , the two regions of extended states merge and a continuum of delocalized states appears around the middle of the magnon spectrum. For this range of dilutions the Chern number seems to be ill defined in the thermodynamic limit, and only for  $p > p_2^*$ , when all states become localized, the system shows  $C = 0$  as expected for a trivial phase. Replacing magnetic with non-magnetic atoms in a systems hosting a magnon Chern insulator in the clean limit puts all the three phases within experimental reach.

## I. INTRODUCTION

Electronics based on the spin degree of freedom (Spintronics) harbor well-known advantages from the present silicon-based technologies [1]. Magnonics [2], a subfield of Spintronics, addresses the use of spin waves (magnons) to transmit and process information [3–6]. By replacing charge currents by spin currents, it is possible to avoid Joule heating, making these technologies of great practical interest [7]. These waves have already been measured in Yttrium Iron Garnet thin-films (YIG) [8]. On the other hand, the study of magnons furnishes fundamental insight about collective excitations and low-energy properties of quantum magnetic systems.

The observation of the anomalous thermal Hall Effect for magnons – intrinsic transverse heat transport response to a longitudinal temperature gradient – in the insulating ferromagnet  $\text{Lu}_2\text{V}_2\text{O}_7$  with a pyrochlore structure [9, 10], and more recently in a Kagomé magnet [11], confirmed that magnonic systems may host topological properties [12] just like other systems with bosonic quasiparticles, such as photons [13] and phonons [14]. Topology was first introduced to condensed matter systems through the 2D electron gas in the quantum Hall regime [15] and through the electronic models of Haldane [16] and Kane-Mele [17] in the honeycomb lattice.

Soon after, topological insulators, a novel type of materials characterized by an insulating bulk and metallic boundary states, became a hot spot of research for their exotic properties and possible applications [18–20]. The presence of edge states in these materials is ensured by the bulk-edge correspondence, a topological property which dictates that edge states properties are deeply connected to the bulk and its symmetries. For small disorder which does not break essential symmetries, these edge states are immune to back-scattering making them the ideal transport states [21, 22]. In the case of neutral quasi-particles such as magnons, the non trivial topology may come from the spin-orbit interaction, imposed by Dzyaloshinskii-Moriya (DM) [23, 24] contribution to the exchange interaction between localized magnetic moments.

A key property of topological insulators is their robustness to moderate disorder [25–27], making them attractive for real applications where disorder cannot be avoided. Disorder may even be an essential ingredient for the experimental observation of a topological response, as is the case of the quantum Hall effect [28]. In some cases, disorder may also benefit the appearance of topological properties in regimes where the unperturbed model is trivial. The topological Anderson insulator is a well known example of this class [29–31], which has

recently been realized in cold atoms [32], photonic crystals [33], and electrical circuits [34]. Disorder induced nontrivial topology has also been proposed [35–40] and observed [41] in higher-order topological insulators. For topological magnon insulators, however, the role of disorder has been much less appreciated.

A particularly interesting type of disorder in magnetic systems is dilution, which can be achieved by replacing a certain fraction  $p$  of magnetic atoms by non-magnetic ones. Diluted quantum magnets have been studied previously, both diluted ferromagnets [42] and antiferromagnets [43]. Since long range order is limited by the classical percolation threshold of the underlying lattice, the question then was whether a quantum phase transition could be induced by dilution prior to the expected classical percolation transition. This question is even more relevant in 2D due to the low dimensionality, but a stochastic series expansion approach for the diluted 2D antiferromagnetic Heisenberg model clearly showed that the percolating cluster at  $p_c$  (the critical classical dilution threshold) showcases long-range order [44, 45]. It was later shown that critical exponents involving dynamical correlations are different from the classical percolation values, even though the transition is driven by the underlying classical percolation [46].

In this article we study the interplay between non-trivial topology and magnetic dilution in 2D topological magnon insulators. We address in particular the question of whether a topological transition takes place with increasing dilution and whether or not there is a relation with the classical percolation threshold of the underlying lattice. Since topological properties are deeply related with localization and transport properties, we also study the effect of dilution on localization of the magnon states. Moreover, dilution falls in the strong disorder classification even for small percentages of vacancies. There is no consensual answer to whether localization properties for this type of disorder follow a one parameter scaling theory [47], like other types of disorder such as Anderson disorder [48]. Using the analysis of the transmission coefficient associated to a simple nearest neighbor model in a diluted lattice, it was shown that for increasing disorder and for a fixed finite energy, the system undergoes a transition from delocalized states to power-law localized states, and for large dilution the system is exponentially localized [49, 50]. We anticipate that the complexity of the localization properties for this type of disorder may introduce interesting topological behaviors.

The paper is organized as follows: In Sec. II, we introduce the model and the methods used to characterize the system. The topological, spectral, and localization properties are discussed in Sec. III. In Sec. IV we provide a thorough discussion of the obtained results. The key results are summarized in Sec. V and some conclusions are drawn. In Appendix A we compute the classical site percolation threshold  $p_c$  for the diluted honeycomb

lattice with first and second neighbor connections.

## II. MODEL AND METHODS

### A. Magnons Model

#### 1. Clean case

We consider the Heisenberg model for localized spins with DM [23] and Zeeman exchange interaction for a ferromagnetic system in the honeycomb lattice with the Hamiltonian written as

$$\mathcal{H} = J \sum_{\langle ij \rangle} \mathbf{S}_i \cdot \mathbf{S}_j + \sum_{\langle\langle ij \rangle\rangle} \mathbf{D}_{ij} \cdot [\mathbf{S}_i \times \mathbf{S}_j] - B \sum_i S_i^z, \quad (1)$$

where  $\langle \dots \rangle$  and  $\langle\langle \dots \rangle\rangle$  refers respectively to the summation over the NN and NNN elements of the lattice and the coupling  $\mathbf{D}_{ij}$  in the honeycomb lattice is given by  $\nu_{ij} D \hat{z}$ , with  $\nu_{ij} = 2/\sqrt{3} (\mathbf{d}_1 \times \mathbf{d}_2) \cdot \mathbf{z} = \pm 1$ , where  $\mathbf{d}_1, \mathbf{d}_2$  are two unit vectors along the bonds connecting the NNN  $\langle\langle i, j \rangle\rangle$ . In the following analysis we fix  $\hbar = 1$ . Considering the low temperature regime, it is possible to study this model by focusing on deviations from the ferromagnetic ground state, and using Holstein-Primakoff formalism [51] to define the creation ( $a_i^\dagger$ ) and annihilation ( $a_i$ ) bosonic operators associated to spin deviations  $a_i^\dagger a_i = n_i = S - S_i^z$ , where  $n_i$  is the number operator of the site  $i$ . The spin operators may then be rewritten as

$$\begin{aligned} S_i^- &= \sqrt{2S} a_i^\dagger \sqrt{1 - \frac{a_i^\dagger a_i}{2S}} \approx \sqrt{2S} a_i^\dagger \\ S_i^+ &= \sqrt{2S} \sqrt{1 - \frac{a_i^\dagger a_i}{2S}} a_i \approx \sqrt{2S} a_i, \end{aligned} \quad (2)$$

where we only kept the zeroth order term, disregarding interactions between bosons, since we will focus only in the low energy regime where  $a_i^\dagger a_i \ll 2S$ , the linear spin-wave approximation. Bosonic statistics do not have a limit on the occupation factor, however, in this approximation the maximum occupation number cannot exceed the number of deviations needed to surpass the minimum spin value.

We can rewrite the Hamiltonian with respect to bosonic operators as

$$\begin{aligned} \mathcal{H} = & 2JS \sum_{\langle ij \rangle} \left( a_i^\dagger a_i - a_i^\dagger a_j \right) \\ & + 2iSD \sum_{\langle\langle ij \rangle\rangle} \nu_{ij} a_i^\dagger a_j - B \sum_i a_i^\dagger a_i, \end{aligned} \quad (3)$$

where we have omitted the constant term associated to the ferromagnetic ground state energy. Making use of translational invariance to write  $\mathcal{H}$  in the momentum basis, it is possible to show that the spectrum of the model follows the dispersion relation

$$E(\mathbf{k}) = 2JS \left( 3 \pm \sqrt{|f(\mathbf{k})|^2 + m(\mathbf{k})^2} \right), \quad (4)$$

where

$$m(\mathbf{k}) = -2\frac{D}{J} (\sin(\mathbf{k} \cdot \mathbf{b}_1) - \sin(\mathbf{k} \cdot (\mathbf{b}_1 - \mathbf{b}_2)) - \sin(\mathbf{k} \cdot \mathbf{b}_2))$$

$$f(\mathbf{k}) = 1 + \exp(i\mathbf{b}_1 \cdot \mathbf{k}) + \exp(i\mathbf{b}_2 \cdot \mathbf{k}), \quad (5)$$

$\mathbf{b}_1, \mathbf{b}_2$  being the reciprocal lattice vectors.

### 2. Non-trivial topology in the clean limit

It becomes clear in Eq. (3) that in the lowest order spin-wave approximation the system is described by a single-particle tight binding model. Apart from the absence of a trivial mass, this bosonic model is equivalent to the fermionic system introduced by Haldane [16], hosting topological phases characterized by the topological index Chern number  $C$ . Given an eigenstate  $|\Psi_{\mathbf{k}}^n\rangle$  of our system associated to the band  $n$ , the Berry curvature may be defined as

$$\Omega_{xy}^{(n)}(\mathbf{k}) = -2\text{Im} \left( \left\langle \partial_{k_x} \Psi_{\mathbf{k}}^n \left| \partial_{k_y} \Psi_{\mathbf{k}}^n \right. \right\rangle \right). \quad (6)$$

The Chern number corresponds to the integral of Berry curvature in Eq. (6) over the first Brillouin zone,

$$C_n = \frac{1}{2\pi} \iint_{1ZB} \Omega_{xy}^n d^2\mathbf{k}. \quad (7)$$

In the trivial phase, both bands have a null Chern number while in the topological phase the valence and conduction band have  $C = \pm 1$ , keeping the overall Chern number null.

Even though this model is a bosonic model and the notion of band filling does not apply like in the equivalent fermionic model, the topological properties of a non-interacting system depend exclusively on the single particle Hamiltonian, which is independent of the statistical descriptions of the particles which inhabit the model. In the bosonic case, the transport properties at low temperature will not be described by the states at the middle of the spectrum, but one can always force an excitation to have a certain energy with a external stimulus. For example, it is possible to excite the edge states in a magnon model, provided that the system is in a topological phase [52–54].

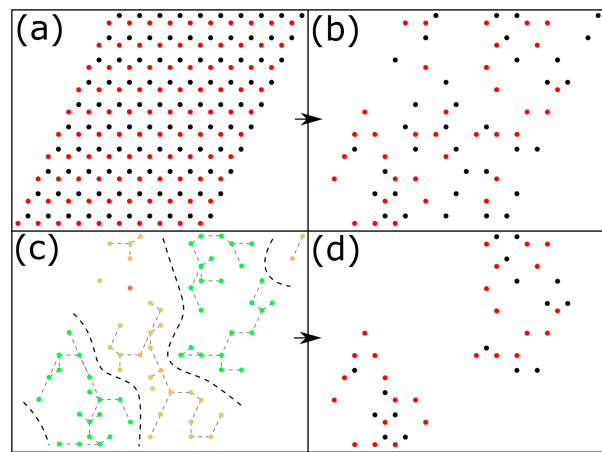


FIG. 1. To obtain the largest cluster of a diluted lattice, we start from a clean honeycomb lattice (a), where the red and black colors make the bipartite nature of the lattice explicit. Running through all the sites in the lattice, we randomly assign the site as vacant with probability  $p$  and in this case we remove it from our graph (b). After choosing all the vacant sites, we collect the different clusters of disconnected sites, as shown in panel (c) with different colors. The model we will consider has next-to-nearest neighbors hoppings, hence we consider that for 2 sites to belong to the same cluster they should be either first neighbors or second neighbors, considering periodic boundary conditions. From all the clusters, we retain just the one with more sites and encode it in a tight binding Hamiltonian (d).

### 3. Diluted Magnons

Diluted lattices are simulated by assuming that each site is independently and randomly occupied with a localized spin with probability  $1 - p$  and it is empty with probability  $p$ . Whenever a site is assigned as a vacancy, it is removed from the tight binding basis. A *cluster* is defined as a set of occupied neighboring sites, which in the terminology of graph theory represents a connected graph. In the spirit of the tight binding approach, we define the neighborhood (set of edges of one vertex) of a site as the set of occupied sites which share non-zero hopping terms. In every disorder configuration we choose random occupied sites and in the end retain solely the largest connected cluster since this will be the one with physical relevance. After collecting the cluster, we build the Hamiltonian of the system with the basis of atomic orbitals of occupied sites only belonging to the largest connected cluster.

Periodic boundary conditions must be employed in order to calculate bulk properties. This modification of the lattice implies occupied sites in two distinct boundaries may still be connected and belong to the same cluster, as exemplified in Fig. 1. A complete finite size honeycomb lattice is shown in Fig. 1(a). In Fig. 1(b) we assign randomly the vacant sites, and in Fig. 1(c) we cluster the

disjoint sets of sites. By keeping only the largest set of sites we obtain the largest connected cluster, shown in Fig. 1(d).

As one increases the percentage of vacancies in the simulated lattice, for percentages larger than a critical value, the size of the largest cluster no longer scales with the same dimensionality as the size of the clean system. It is not possible to take the thermodynamic limit for  $p > p_c$ , as the simulated system has no dependence on the original size of the clean system. This critical value is the so-called classical percolation threshold  $p_c$  and only depends on the lattice geometry [55, 56]. A second and equivalent definition of this quantity, which highlights the physical relevance of this property, is the following: the probability of having a macroscopic path composed of connected sites on a simulated diluted lattice is 0 if  $p > p_c$  and is 1 if  $p < p_c$ . This implies that there is no transport nor long range order for  $p > p_c$ . Although the classical percolation threshold for the honeycomb lattice with nearest neighbors connections is well known to be  $p_c \approx 0.302957$  [55], there are no results in the literature for the honeycomb with first and second nearest neighbors connections. We determined this value to be  $p_c = 0.640 \pm 0.005$  (see Appendix A).

In the diluted regime, the Hamiltonian is rewritten as

$$\mathcal{H} = 2JS \sum_{\langle ij \rangle} \eta_i \eta_j (a_i^\dagger a_i - a_i^\dagger a_j) + 2iSD \sum_{\langle\langle ij \rangle\rangle} \eta_i \eta_j \nu_{ij} a_i^\dagger a_j - B \sum_i \eta_i a_i^\dagger a_i, \quad (8)$$

where dilution is introduced in the Hamiltonian with the random variables  $\eta_i$ , which take the values 0 or 1 depending whether the site  $i$  exists in the lattice being simulated or not. Notice that the first term of the Hamiltonian in Eq. (8) introduces a dependency on the number of occupied neighbors of one site to the respective on-site energy, which is not present in the Haldane model. In this work we fixed  $2JS \equiv t$ ,  $2SD = 0.1t$ ,  $B = 0$ , and use  $t$  as the energy unit.

Disorder breaks translational invariance, meaning that the Hamiltonian eigenstates will no longer be Bloch states with well defined Bloch momentum and band index. Nevertheless, it is still possible to extend the formalism applied in undiluted systems, and compute the Chern number with a real space approach, as discussed next.

## B. Methods

### 1. Chern number

The computation of the Chern number can be extended to systems with broken translational invariance

employing a super-cell approach with twisted boundary conditions in real space. With Fukui's method [57], one can replace the continuous integral in Eq. 7 by a discrete sum over boundary twists  $\theta$ . Additionally, with the coupling matrix method of Ref. [58], we can reduce the sum to twist angles associated to periodic boundary conditions. This method requires exact diagonalization of two matrices with size proportional to the system's size: the Hamiltonian, and the coupling matrix [58].

To minimize finite size effects, we average the Chern number over disorder realizations. Even though the Chern number is strictly quantized for each disorder configuration, the averaged Chern number may not be. A finite size scaling analysis is performed when needed in order to infer the thermodynamic limit behavior.

### 2. Density of states

In order to build the gapless-gapped picture for the model, we used the Kernel Polynomials Method (KPM) [59] to compute the density of states through a Chebyshev polynomials series expansion, equipped by the Jackson's Kernel. The linear scaling of this method with the system size allowed us to explore systems of the order of  $N = 1024^2$  unit cells.

A finite cutoff of the series expansion introduces an artificial smoothing in abrupt changing parts of the spectrum, which may lead to wrong interpretations about the existence of a gap for small enough gaps. In these cases, an analysis of the convergence of the DOS in the gap with respect to the cutoff order of the series expansion was employed in hopes of minimizing the uncertainty of the limits of the gapped-gapless phases.

### 3. Localization

The localization behavior of the system was explored using the standard tools: level spacing statistics [60] to try to observe a transition from a GUE (Gaussian Unitary Ensemble) distribution to a Poisson distribution as states become localized, and Transfer Matrix Method (TMM) [28] to compute the scaling of the correlation/localization length across the spectrum for different dilution percentages.

In order to identify the probability distribution of the level spacings, we looked at the distribution of the ratio between consecutive level spacings,  $r_n = \min(s_n, s_{n+1}) / \max(s_n, s_{n+1})$ , where  $s_n = \epsilon_{n+1} - \epsilon_n$  are the level spacings. This quantity is known to have better behavior in regions of the spectrum with low density of states [61, 62].

In order to implement the TMM, we had to assign a high on-site energy  $V_{\text{vacancy}}$  to the vacant sites, plus a very small hopping term  $\delta t$  from adjacent sites to these

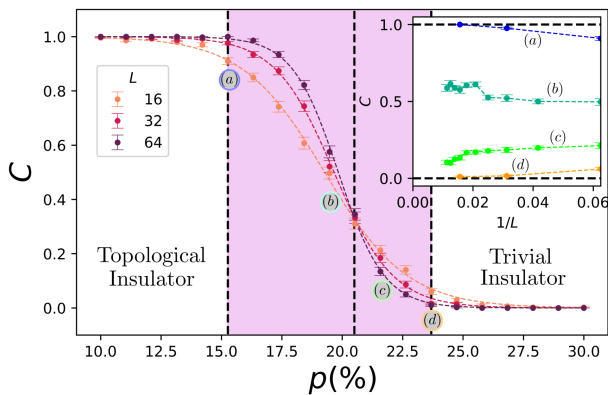


FIG. 2. Averaged Chern number for different system sizes ( $L$  is the total number of unit cells in one spacial direction) and for different percentages of vacancies. The standard deviation errors obtained by averaging over 500 disorder realizations are shown for each data point. Inset: finite size scaling analysis for the averaged Chern number at specific dilution values:  $p = 15.3\%$  (a),  $p = 19.5\%$  (b),  $p = 21.6\%$  (c), and  $p = 23.7\%$  (d).

vacant sites, instead of removing the vacant sites from our tight binding basis. We used  $V_{\text{vacancy}} = 1000t$  and  $\delta t/t = 1/1000$ . The limit  $V_{\text{vacancy}} \rightarrow \infty, \delta t \rightarrow 0$ , where both implementations of dilution should be equivalent, is discussed in Sec. IV.

### III. RESULTS

#### A. Topological phase diagram

As can be seen in Fig. 2, the topological phase is robust up to relatively high percentages of vacancies, persisting with a well defined Chern number  $C = 1$  up to  $p \approx 15\%$ . In the inset of Fig. 2 it is clearly seen that for  $p = 15.3\%$ , labeled with (a) in the inset, we have an averaged Chern number  $C \rightarrow 1$  as  $1/L \rightarrow 0$ . For large enough dilution, which we overestimate as  $p \gtrsim 23\%$ , the system enters the trivial phase. In this region of the phase diagram  $C \rightarrow 0$  as  $1/L \rightarrow 0$ , as shown for  $p = 23.7\%$ , labeled with (d) in the inset of Fig. 2. The system becomes a trivial insulator before reaching the classical percolation threshold for the honeycomb lattice,  $p_c = 30\%$ , and long before the threshold for the honeycomb lattice with first and second nearest neighbors,  $p_c = 64\%$ , rendering the trivial phase physically achievable.

Between the topological and the trivial phases shown in Fig. 2, there is a highlighted region for  $15\% \lesssim p \lesssim 23\%$  where the averaged Chern number crosses over from  $C = 1$  to  $C = 0$  as  $p$  increases. Our numerical analysis is not conclusive on whether this region shrinks to a single critical dilution in the thermodynamic limit or remains finite. Nevertheless, a finite size scaling analysis seems to indicate that the averaged Chern number

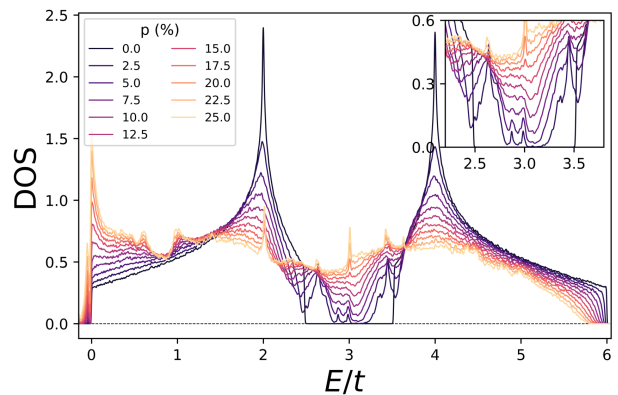


FIG. 3. DOS for different percentages of dilution, including both the topological and the trivial phases, as well as the crossover region. We used systems with size  $1024 \times 1024$  and included 1024 polynomials in the KPM.

does not converge to quantized values as we approach the thermodynamic limit. This is exemplified in the inset of Fig. 2 for  $p$  values labeled with (b) and (c). The presence of a crossover region which does not shrink to a single critical dilution is also justified by the localization behavior of the system to be discussed in Sec. III B 2.

#### B. Spectral and localization properties

##### 1. Spectral properties

In Fig. 3 we show the magnon DOS for different values of dilution  $p$  obtained using KPM. It is obvious that even for a small percentage of vacancies (above  $p \simeq 5\%$ ) the gap is completely filled. This implies that the topological phase becomes gapless for small values of dilution. The gap remains closed as disorder increases, even when the system becomes trivial.

The diagonal disorder seen in Eq. (8) destroys the particle-hole symmetry of the spectrum for finite dilution, something that does not appear in analogous fermionic systems, like the Haldane model. This asymmetry shifts the middle of the spectrum to lower energies as dilution increases.

##### 2. Localization properties

In order to provide a more complete analysis of the topological phase transition, we have also characterized the localization properties of the system for different values of  $p$ . The ratio between consecutive level spacings  $r_n$ , introduced in Sec. II B 3, allows to distinguish between localized and extended states. For localized states  $r_n$  should follow the Poisson distribution, while for extended states in systems which break time reversal sym-

metry we expect the Gaussian Unitary Ensemble (GUE) distribution [60].

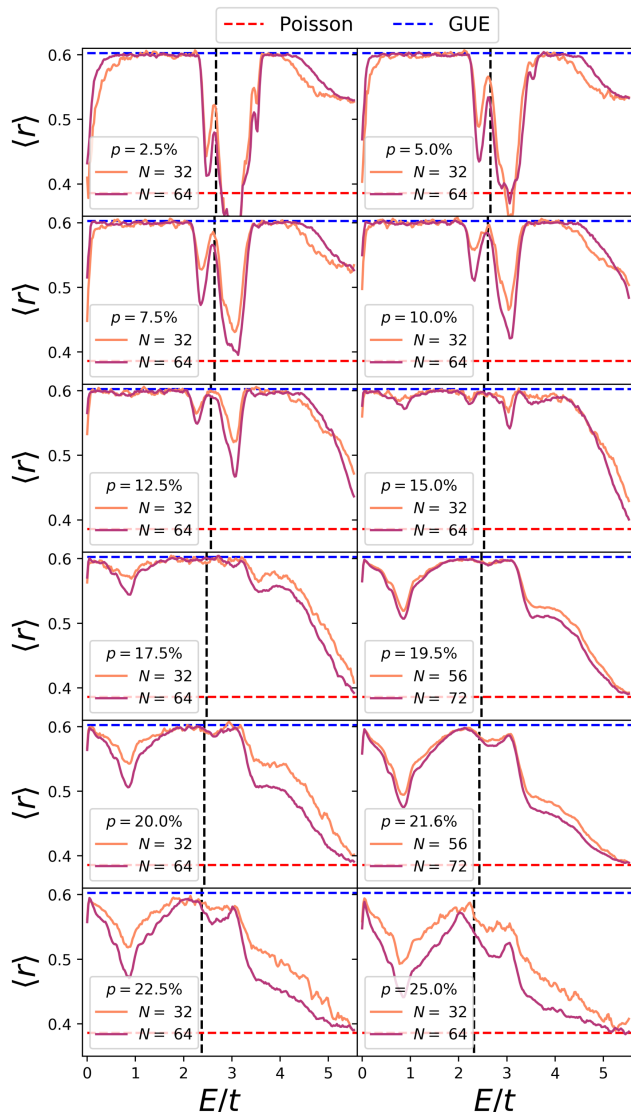


FIG. 4. Finite size scaling for the average value  $\langle r \rangle$  of the distribution of the ratio between consecutive energy spacings as a function of energy for increasing values of dilution percentages  $p$ . We compare this average with the one expected for the GUE (horizontal dashed blue line) and Poisson distribution (horizontal dashed red line). The vertical dashed black line marks the middle of the spectrum, marking also the upper limit of integration of the Berry curvature. The statistics are averaged over a total number of 2048 realizations of disorder for  $N = 32^2$  and 256 realizations of disorder for  $N = 64^2$ , and the bin's size used for the statistics is of the order of  $0.05t$ .

In Fig. 4 we show the first moment of the distribution,  $\langle r \rangle$ , indicating as dashed horizontal lines the expected values for the Poisson and GUE distributions. With increasing dilution up to  $p \lesssim 15\%$ , there are two persistent regions, one below the middle of the spectrum (signaled by the vertical dashed line) and the other above

it, where  $\langle r \rangle$  seems to converge to GUE with increasing system size. These two regions are separated by a region of localized states around the middle of the spectrum, where  $\langle r \rangle$  is converging to the Poisson value. The presence of two finite energy regions where states are delocalized is at odds with the behavior of quantum Hall systems [28, 63] and conventional Chern insulators [31, 64–66], where extended states appear only at isolated single energies. However, site dilution (or vacancies) is a particular type of disorder where unconventional behavior is to be expected [49, 50]. Yet another important remark to be made is the presence of localized states around the middle of the spectrum, separating the two regions of extended states. Since the spectrum is gapless in the topological phase, it is the feature of having localized states filling the gap which allows the system to retain the topological properties reminiscent from the clean system.

If we further increase the percentage of vacancies, it can be seen in Fig. 4 that for  $15\% \lesssim p \lesssim 23\%$  the states previously localized for smaller  $p$  values become extended, forming a continuum of extended states around the middle of the spectrum. We believe this continuum to be responsible for the crossover behavior observed in Fig. 2 regarding the topological character of the system. The presence of this continuum prevents the usual “levitation and pair annihilation” of the extended states carrying the topological index [65, 67, 68] and the existence of critical dilution at which the topological transition would take place. As soon as dilution reaches the trivial phase, all the spectrum becomes localized as is possible to observe in Fig. 2 for  $p = 25\%$ .

In order to enrich our conclusions regarding the localization properties, we computed the localization length with the TMM. As can be seen in Fig 5, for small dilution up to  $p \lesssim 15\%$  we observe two regions in which the normalized localization length  $\Lambda_M$  is scale invariant, corresponding to delocalized states. These two regions are separated by a region where  $\Lambda_M$  decreases with  $M$ , signaling the presence of localized states. This agrees well with the level spacing statistics results of Fig. 4. In the crossover region  $15\% \lesssim p \lesssim 23\%$ , we also see the presence of a continuum of extended states spanning a large region around the middle the spectrum (note the collapse of  $\Lambda_M$  for the larger  $M$  values). This confirms the unconventional localization properties of this system when compared with conventional disordered Chern insulators [31]. Upon reaching the trivial phase, all the states become localized, as is possible to observe for  $p \gtrsim 23\%$ , where  $\Lambda_M$  decreases with the transverse size of the system,  $M$ , for the entire spectrum. Even though the TMM results and those from level spacing statistics are in qualitative agreement, there are noticeable quantitative differences which we discuss in Sec. IV.

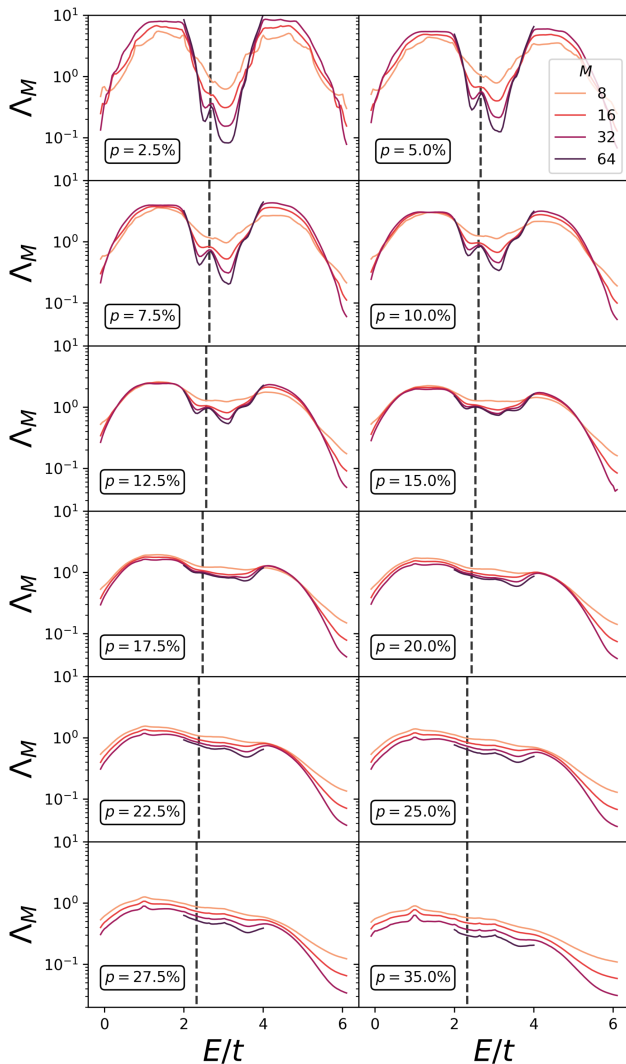


FIG. 5. Finite size scaling analysis of the normalized localization length  $\Lambda_M$  with the transverse size of the ribbon  $M$  in the TMM for different concentrations of vacancies. The longitudinal length used ensures that the estimated error had converged to under 1%. The energy resolution is of the order of  $0.05t$ .

### 3. Spin-wave stability

As dilution increases, a finite density of states with negative energies appears very close to zero, as can be clearly seen in Fig. 3. Negative energy eigenstates would imply that the ferromagnetic state is not the true ground state of the system, rendering the usage of Holstein-Primakoff transformation not valid. This problem can be easily surpassed by making use of a finite magnetic field, which would make a rigid shift of the spectrum. This shift would open a energy gap between the ferromagnetic state and the lowest energy excitations, thus stabilizing the spin-waves. The presence of single-ion magnetic anisotropy would also give rise to a term in

the Hamiltonian with similar effects.

## IV. DISCUSSION

The unconventional localization properties in the crossover region support the conjecture that a topological index cannot be defined for this range of dilutions since the system has delocalized magnons in a large window around the middle of the spectrum (equivalent to a metallic phase in fermionic systems). This is in agreement with the results of Fig 2 for the averaged Chern number in the crossover region, which does not seem to converge to a quantized value. The topological to trivial phase transition occurs when the localized states, which separate the energy windows with extended states, become localized. As dilution is increased, this enables a continuous flow of Berry curvature between the two regions with delocalized states. We speculate that the presence of a smooth crossover transition occurs because of the appearance of this continuum near the transition.

In fermionic models belonging to the same symmetry class similar behavior was already observed: the transition from the topological phase to the trivial one on increasing disorder occurs through a metallic phase [69–72], for a finite range of disorder values and not at a single critical disorder. The key point to obtain the metallic behavior in these works is the presence of spin-flip hopping disorder. Even though a clear relation between this latter type of disorder and dilution is hard to establish, we notice that, in the clean limit, the two sublattices of the honeycomb lattice ensure a two-component wavefunction similar to spin-1/2 systems; around the middle of the spectrum it is even possible to define a pseudo-spin from the sublattice degree of freedom [73]. Pushing forward the connection, nearest neighbor hopping disorder would mix the two components of the wave function in a similar way as spin-flip processes mix spin-up and spin-down. Finally, dilution may be regarded as an extreme case of hopping disorder, where certain random hoppings are set to zero.

Another point worth mentioning is the reason for some quantitative differences between the results from the TMM in Fig. 5 and the level spacing statistics in Fig. 4. In the level spacing statistics we make use of exact diagonalization of the Hamiltonian associated solely to the largest cluster for a given configuration of vacancies, while for the TMM we cannot remove the small isolated clusters from the computation. This means that this second method opens the possibility of hosting for the same energy value, both localized states in the independent clusters and localized states over the physical cluster, which hybridize through the small hopping used to simulate vacancies (see Sec. II B 3). We believe this to be the reason for the absence of scaling of  $\Lambda_M$  with  $M$  in sections of the spectrum for which the level spacing

statistics seems to tell us unambiguously that we are in the presence of localized states (example around  $E = 4t$  for dilutions in the crossover region).

## V. CONCLUSIONS

In this work we have studied the effect of magnetic dilution in a system which hosts, in the clean limit, a topological magnon insulating phase. We have shown that the topological phase is robust to the presence of magnetic vacancies, surviving with a well defined Chern number  $C = 1$  up to a moderate dilution  $p_1^*$ , which for the considered model we estimate to be around  $p_1^* \approx 15\%$ . For high enough dilution  $p_2^* > p_1^*$ , the system enters a trivial phase with  $C = 0$ . For the considered model we estimate  $p_2^* \approx 23\%$ . Interestingly, we found  $p_1^*, p_2^* < p_c$ , where  $p_c$  is the classical percolation threshold, which for the honeycomb lattice with nearest neighbor connections is  $p_c \simeq 30\%$  (taking into account the second neighbor connections present in our model it is  $p_c \simeq 64\%$ ).

Through an extensive characterization of the localization properties, we have established that for  $p < p_1^*$ , when the system is in the topological phase, the states that fill the clean limit gap are localized. The system behaves effectively as a topological Chern insulator, with Berry curvature carried by two energy regions of extended states above and below the region of localized states. For  $p > p_2^*$ , when the system is in the trivial phase with  $C = 0$ , all states are localized. In the crossover region, for  $p_1^* < p < p_2^*$ , we have found a continuum of extended states (possibly critical) around the middle of the spectrum, in the region previously occupied by the localized states in the topological phase for  $p < p_1^*$ . Based on the localization properties and a finite scaling analysis of the Chern number, we conjecture that, in the thermodynamic limit, the topological index is not well defined in this region and topological properties are not to be expected for  $p_1^* < p < p_2^*$ .

Replacing magnetic atoms with non-magnetic ones in a systems hosting a magnon Chern insulator in the clean limit puts all the three phases within experimental reach. Although most 2D ferromagnetic honeycomb materials, like the compounds  $\text{CrX}_3$  ( $X \equiv \text{Cl, I}$  and  $\text{Br}$  [74–78]), do not exhibit a strong enough DM interaction to originate nontrivial behavior, it is possible to mimic this interaction with the use of an external time dependent electric field [79] or to increase the existing interaction via structural changes in the compound such as strain [80] and the addition of more layers [81], allowing the clean limit topological properties to be engineered [82]. An interesting open question is whether dilution in topological kagome ferromagnets leads to qualitatively similar physics [83, 84].

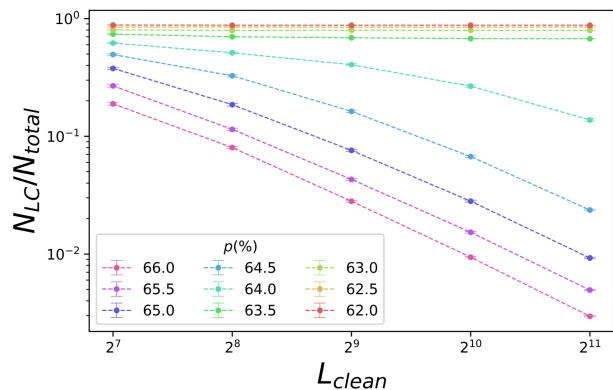


FIG. 6. Fraction of sites belonging to the largest cluster as a function of the clean system size in one spacial direction for different values of  $p$  averaged over 300 configurations of dilution.

## ACKNOWLEDGEMENTS

MSO and EVC acknowledge partial support from Fundação para a Ciência e Tecnologia (FCT-Portugal) through Grant No. UIDB/04650/2020. NMRP acknowledges support from the Independent Research Fund Denmark (grant No. 2032-00045B), the Danish National Research Foundation (Project No. DNRF165) and Fundação para a Ciência e Tecnologia (FCT-Portugal) through Grant No. PTDC/FIS-MAC/2045/2021.

### Appendix A: Classical percolation problem

In order to compute the classical site percolation threshold  $p_c$  for the diluted graphs where the vertices are the honeycomb lattice points and the first and second neighbors are the edges, we computed the fraction of sites which belong to the largest cluster of a simulated lattice for different clean system sizes and for different percentages of vacancies. The results in the Fig. 6 seem to indicate that for percentages below 64%, the fraction of sites in the largest cluster is constant with respect to the increase of the system size, and for percentages higher than 64% there is a clear scaling with  $\propto 1/N_{\text{total}}$  showing that the largest cluster has a constant size for these percentages. We estimate the value of  $p_c$  to be around 64% since we have the transition from the two distinct behaviors at this point.

### Appendix B: Level spacing statistics sampling

For each disorder configuration, we obtained the set of energies,  $e_n$ , with exact diagonalization. With this set, we computed the energy spacings between consecutive levels,  $s_n = e_n - e_{n-1}$ , and used them to calculate

the ratio between consecutive energy spacings defined as  $r_n = \min(s_n, s_{n+1}) / \max(s_n, s_{n+1})$ . This last quantity is known to behave better in regions where the DOS is small [61, 62]. After gathering the lists of  $r_n$  over several dilution configurations, we grouped them in equally spaced bins over the spectrum to compute the average ratio  $\langle r \rangle$  inside each bin and obtain  $\langle r \rangle$  as a function of energy and compare it with the expected result for the GUE and Poisson distributions (Fig. 4). The bin size was chosen small enough so we could probe the principal changes in localization properties along the topological transition, but large enough to enable  $\langle r \rangle$  to have a smooth behavior.

- 
- [1] P. J. Rajput, S. U. Bhandari, and G. Wadhwa, *Silicon* (2022), [10.1007/s12633-021-01643-x](https://doi.org/10.1007/s12633-021-01643-x).
- [2] B. Lenk, H. Ulrichs, F. Garbs, and M. Münzenberg, *Physics Reports* **507**, 107 (2011).
- [3] A. A. Serga, S. O. Demokritov, B. Hillebrands, and A. N. Slavin, *Physical Review Letters* **92**, 117203 (2004).
- [4] V. E. Demidov, M. P. Kostylev, K. Rott, P. Krzysteczko, G. Reiss, and S. O. Demokritov, *Applied Physics Letters* **95**, 112509 (2009).
- [5] J. Jorzick, S. O. Demokritov, B. Hillebrands, M. Bailleul, C. Fermon, K. Y. Guslienko, A. N. Slavin, D. V. Berkov, and N. L. Gorn, *Physical Review Letters* **88**, 047204 (2002).
- [6] J. Podbielski, F. Giesen, and D. Grundler, *Physical Review Letters* **96**, 167207 (2006).
- [7] A. Barman, G. Gubbiotti, S. Ladak, A. O. Adeyeye, M. Krawczyk, J. Gräfe, C. Adelman, S. Coto-fana, A. Naeemi, V. I. Vasyuchka, B. Hillebrands, S. A. Nikitov, H. Yu, D. Grundler, A. V. Sadovnikov, A. A. Grachev, S. E. Sheshukova, J.-Y. Duquesne, M. Marangolo, G. Csaba, W. Porod, V. E. Demidov, S. Urazhdin, S. O. Demokritov, E. Albisetti, D. Petti, R. Bertacco, H. Schultheiss, V. V. Kruglyak, V. D. Poimanov, S. Sahoo, J. Sinha, H. Yang, M. Münzenberg, T. Moriyama, S. Mizukami, P. Landeros, R. A. Gallardo, G. Carlotti, J.-V. Kim, R. L. Stamps, R. E. Camley, B. Rana, Y. Otani, W. Yu, T. Yu, G. E. W. Bauer, C. Back, G. S. Uhrig, O. V. Dobrovolskiy, B. Budinska, H. Qin, S. van Dijken, A. V. Chumak, A. Khitun, D. E. Nikonov, I. A. Young, B. W. Zingsem, and M. Winklhofer, *Journal of Physics: Condensed Matter* **33**, 413001 (2021).
- [8] M. B. Jungfleisch, W. Zhang, W. Jiang, H. Chang, J. Sklenar, S. M. Wu, J. E. Pearson, A. Bhattacharya, J. B. Ketterson, M. Wu, and A. Hoffmann, *Journal of Applied Physics* **117**, 17D128 (2015), <https://doi.org/10.1063/1.4916027>.
- [9] Y. Onose, T. Ideue, H. Katsura, Y. Shiomi, N. Nagaosa, and Y. Tokura, *Science* **329**, 297 (2010), arXiv:1008.1564 [cond-mat].
- [10] M. Hirschberger, J. W. Krizan, R. Cava, and N. Ong, *Science (New York, N.Y.)* **348**, 106–109 (2015).
- [11] M. Hirschberger, R. Chisnell, Y. S. Lee, and N. P. Ong, *Phys. Rev. Lett.* **115**, 106603 (2015), arXiv:1502.05688.
- [12] R. Chisnell, J. S. Helton, D. E. Freedman, D. K. Singh, R. I. Bewley, D. G. Nocera, and Y. S. Lee, *Physical Review Letters* **115**, 147201 (2015).
- [13] G. L. J. A. Rikken and B. A. van Tiggelen, *Nature* **381**, 54 (1996).
- [14] L. Zhang, J. Ren, J.-S. Wang, and B. Li, *Physical Review Letters* **105**, 225901 (2010).
- [15] D. J. Thouless, M. Kohmoto, M. P. Nightingale, and M. den Nijs, *Physical Review Letters* **49**, 405 (1982), arXiv:arXiv:1011.1669v3.
- [16] F. D. M. Haldane, *Phys. Rev. Lett.* **61**, 2015 (1988).
- [17] C. L. Kane and E. J. Mele, *Physical Review Letters* **95**, 226801 (2005).
- [18] L. Fu, *Physical Review Letters* **104**, 056402 (2010).
- [19] S. Vijay, T. H. Hsieh, and L. Fu, *Physical Review X* **5**, 041038 (2015).
- [20] E. Dennis, A. Kitaev, A. Landahl, and J. Preskill, *Journal of Mathematical Physics* **43**, 4452 (2002), arXiv:quant-ph/0110143.
- [21] J. L. Lado, N. Garcia-Martinez, and J. Fernandez-Rossier, (2015), [10.48550/ARXIV.1502.07112](https://arxiv.org/abs/10.48550/ARXIV.1502.07112).
- [22] S. Murakami, *Journal of Physics: Conference Series* **302**, 012019 (2011).
- [23] T. Moriya, *Physical Review* **120**, 91 (1960).
- [24] P. A. McClarty, *Annual Review of Condensed Matter Physics* **13**, 171 (2022), arXiv:2106.01430.
- [25] B. Wu, J. Song, J. Zhou, and H. Jiang, (2017), [10.48550/ARXIV.1711.10725](https://arxiv.org/abs/10.48550/ARXIV.1711.10725).
- [26] Y. Li, *Nature Physics* **15**, 4 (2019).
- [27] D. Xiao, M.-C. Chang, and Q. Niu, *Reviews of Modern Physics* **82**, 1959 (2010).
- [28] B. Kramer and A. MacKinnon, *Rep. Prog. Phys.* **56**, 1469 (1993).
- [29] C. W. Groth, M. Wimmer, A. R. Akhmerov, J. Tworzydło, and C. W. J. Beenakker, *Physical Review Letters* **103**, 196805 (2009).
- [30] J. Li, R.-L. Chu, J. K. Jain, and S.-Q. Shen, *Physical Review Letters* **102**, 136806 (2009).
- [31] M. Gonçalves, P. Ribeiro, and E. V. Castro, arXiv:1807.11247 [cond-mat, physics:quant-ph] (2018), arXiv:1807.11247.
- [32] E. J. Meier, F. A. An, A. Dauphin, M. Maffei, P. Massignan, T. L. Hughes, and B. Gadway, *Science* **362**, 929 (2018).
- [33] S. Stützer, Y. Plotnik, Y. Lumer, P. Titum, N. H. Lindner, M. Segev, M. C. Rechtsman, and A. Szameit, *Nature* **560**, 461 (2018).
- [34] Z.-Q. Zhang, B.-L. Wu, J. Song, and H. Jiang, *Physical Review B* **100**, 184202 (2019), arXiv:1906.04064.
- [35] C. A. Li, B. Fu, Z. A. Hu, J. Li, and S. Q. Shen, *Physical Review Letters* **125**, 166801 (2020), 2008.00513.
- [36] Y.-B. Yang, K. Li, L.-M. Duan, and Y. Xu, *Physical Review B* **103**, 085408 (2021).
- [37] A. Agarwala, V. Juričić, and B. Roy, *Physical Review Research* **2**, 012067 (2020).
- [38] J.-H. Wang, Y.-B. Yang, N. Dai, and Y. Xu, *Physical Review Letters* **126**, 206404 (2021).
- [39] T. Peng, C.-B. Hua, R. Chen, Z.-R. Liu, H.-M. Huang, and B. Zhou, *Physical Review B* **106**, 125310 (2022).
- [40] H. Lóio, M. Gonçalves, P. Ribeiro, and E. V. Castro, (2023), arXiv:2305.19209.
- [41] W. Zhang, D. Zou, Q. Pei, W. He, J. Bao, H. Sun, and X. Zhang, *Physical Review Letters* **126**, 146802 (2020), arXiv:2008.00423.

- [42] S. F. Edwards and R. C. Jones, *Journal of Physics C: Solid State Physics* **4**, 2109 (1971).
- [43] C. C. Wan, A. B. Harris, and J. Adler, *Journal of Applied Physics* **69**, 5191 (1991).
- [44] A. W. Sandvik, *Physical Review Letters* **86**, 3209 (2001).
- [45] A. W. Sandvik, *Physical Review B* **66**, 024418 (2002).
- [46] T. Vojta and J. Schmalian, *Physical Review Letters* **95**, 237206 (2005), [arXiv:0508211](#).
- [47] E. Abrahams, P. W. Anderson, D. C. Licciardello, and T. V. Ramakrishnan, *Physical Review Letters* **42**, 673 (1979).
- [48] P. W. Anderson, *Physical Review* **109**, 1492 (1958).
- [49] M. Islam and H. Nakanishi, *Physical review. E, Statistical, nonlinear, and soft matter physics* **77**, 061109 (2008).
- [50] B. S. Dillon and H. Nakanishi, *The European Physical Journal B* **87** (2014), [10.1140/epjb/e2014-50397-4](#).
- [51] T. Holstein and H. Primakoff, *Physical Review* **58**, 1098 (1940).
- [52] R. Shindou, R. Matsumoto, S. Murakami, and J.-i. Ohe, *Physical Review B* **87**, 174427 (2013).
- [53] L. Zhang, J. Ren, J.-S. Wang, and B. Li, *Physical Review B* **87**, 144101 (2013).
- [54] A. Mook, J. Henk, and I. Mertig, *Physical Review B* **90**, 024412 (2014).
- [55] P. N. Suding and R. M. Ziff, *Physical Review E* **60**, 275 (1999).
- [56] R. M. Ziff, *Physical Review Letters* **69**, 2670 (1992).
- [57] T. Fukui, Y. Hatsugai, and H. Suzuki, *Journal of the Physical Society of Japan* **74**, 1674 (2005).
- [58] Y. F. Zhang, Y. Y. Yang, Y. Ju, L. Sheng, D. N. Sheng, R. Shen, and D. Y. Xing, *Chinese Physics B* **22**, 117312 (2013), [arXiv: 1212.6295](#).
- [59] A. Weiße, G. Wellein, A. Alvermann, and H. Fehske, *Reviews of Modern Physics* **78**, 275 (2006).
- [60] F. Evers and A. D. Mirlin, *Reviews of Modern Physics* **80**, 1355 (2008).
- [61] V. Oganesyan and D. A. Huse, *Physical Review B* **75**, 155111 (2007).
- [62] Y. Y. Atas, E. Bogomolny, O. Giraud, and G. Roux, *Physical Review Letters* **110**, 084101 (2013).
- [63] C. Wang, Y. Avishai, Y. Meir, and X. R. Wang, *Physical Review B* **89**, 45314 (2014).
- [64] M. Onoda and N. Nagaosa, *Physical Review Letters* **90**, 206601 (2003).
- [65] M. Onoda, Y. Avishai, and N. Nagaosa, *Phys. Rev. Lett.* **98** (2007), [10.1103/PhysRevLett.98.076802](#), [0605510](#).
- [66] E. V. Castro, R. de Gail, M. P. López-Sancho, and M. A. H. Vozmediano, *Physical Review B* **93**, 245414 (2016).
- [67] R. B. Laughlin, *Physical Review Letters* **52**, 2304 (1984).
- [68] E. Prodan, *Journal of Physics A: Mathematical and Theoretical* **44**, 113001 (2011), [arXiv:1010.0595](#).
- [69] C. Wang, Y. Su, Y. Avishai, Y. Meir, and X. R. Wang, *Physical Review Letters* **114**, 096803 (2015), [arXiv:1411.4838](#).
- [70] Z. Qiao, Y. Han, L. Zhang, K. Wang, X. Deng, H. Jiang, S. A. Yang, J. Wang, and Q. Niu, *Phys. Rev. Lett.* **117**, 056802 (2016).
- [71] Y. Su, C. Wang, Y. Avishai, Y. Meir, and X. R. Wang, *Scientific Reports* **6**, 33304 (2016).
- [72] H. Yang, J. Zeng, Y. Han, and Z. Qiao, *Physical Review B* **104**, 115414 (2021).
- [73] A. H. Castro Neto, F. Guinea, N. M. R. Peres, K. S. Novoselov, and A. K. Geim, *Reviews of Modern Physics* **81**, 109 (2009), [arXiv:0709.1163](#).
- [74] B. Huang, G. Clark, E. Navarro-Moratalla, D. R. Klein, R. Cheng, K. L. Seyler, D. Zhong, E. Schmidgall, M. A. McGuire, D. H. Cobden, W. Yao, D. Xiao, P. Jarillo-Herrero, and X. Xu, *Nature* **546**, 270 (2017).
- [75] H. L. Davis and A. Narath, *Phys. Rev.* **134**, A433 (1964).
- [76] A. Narath and H. L. Davis, *Phys. Rev.* **137**, A163 (1965).
- [77] E. J. Samuelsen, R. Silbergliitt, G. Shirane, and J. P. Remeika, *Phys. Rev. B* **3**, 157 (1971).
- [78] L. Chen, J.-H. Chung, T. Chen, C. Duan, A. Schneidewind, I. Radelytskyi, D. J. Voneshen, R. A. Ewings, M. B. Stone, A. I. Kolesnikov, B. Winn, S. Chi, R. A. Mole, D. H. Yu, B. Gao, and P. Dai, *Phys. Rev. B* **101**, 134418 (2020).
- [79] S. A. Owerre, *Journal of Physics Communications* **1**, 021002 (2017), [arXiv:1705.04694 \[cond-mat\]](#).
- [80] T. Koretsune, N. Nagaosa, and R. Arita, *Scientific Reports* **5**, 13302 (2015).
- [81] W. Legrand, Y. Sassi, F. Ajejas, S. Collin, L. Bocher, H. Jia, M. Hoffmann, B. Zimmermann, S. Blügel, N. Reyren, V. Cros, and A. Thiaville, *Physical Review Materials* **6**, 024408 (2022).
- [82] T. V. C. Antão and N. M. R. Peres, *Physical Review B* **107**, 235410 (2023), [arXiv:2303.03305](#).
- [83] F. Zhuo, H. Li, and A. Manchon, *Physical Review B* **104**, 144422 (2021).
- [84] F. Zhuo, H. Li, and A. Manchon, *New Journal of Physics* **24**, 023033 (2022).